Energy Conversion and Management 163 (2018) 100–110

Contents lists available at ScienceDirect

Energy Conversion and Management

journal homepage: www.elsevier.com/locate/enconman

A Comparative study on the aeromechanic performances of upwind and downwind horizontal-axis wind turbines

Zhenyu Wang[1], Wei Tian, Hui Hu*

Department of Aerospace Engineering, Iowa State University, Ames, IA 50011, USA

ARTICLE INFO

Keywords:
Upwind turbine (UWT)
Downwind turbine (DWT)
Turbine aeromechanics
Wake flow characteristics

ABSTRACT

Traditional horizontal-axis wind turbines are mainly designed as upwind configuration. In order to avoid blade strikes, the rotor blades have to be positioned far enough away from the turbine tower and have to be designed as inflexible as possible. In addition, a complicated yaw control system is required to keep the turbine rotor facing the incoming wind. Due to these drawbacks, the turbine in downwind configuration is proposed to overcome these disadvantages because, first of all, rotor blades can be designed more flexible since there is no danger of blade strikes, and secondly, yaw control system could be eliminated if nacelle is designed appropriately to follow the incoming wind direction passively. In the present study, a comparative experimental investigation was conducted to quantify the aeromechanic performance of a downwind turbine (DWT), in comparison to that of a traditional upwind turbine (UWT). The thrust coefficient of the DWT model was found to be increased slightly in the time-averaged quantity, but have a significant augment in the fluctuations. Due to the shadow effect, the power outputs of the DWT model was found to be decreased by 3.2% when they were operated in a same atmospheric boundary layer (ABL) wind. In addition, a high-resolution particle image velocimetry (PIV) system was employed to characterize the ensemble-averaged and phase-locked wake flow structures to quantify the turbulent flow characteristics in the turbine wakes. The velocity deficit in the lower half turbine wake for the UWT case was found to be greater than that of the DWT case at the location of $X/D < 1.0$. The higher wind load fluctuations for the DWT system were found to be correlated well with the higher TKE distributions in the turbine wakes. The phase-locked PIV measurements illustrated that the wake regions can be divided into four zones, which are dominated by the vortices shedding from different turbine components. The detailed flow field measurements were correlated with the dynamic force and power measurement data to elucidate the underlying physics.

1. Introduction

Wind energy is one of the primary renewable and clean energy sources. Wind turbines are the most common system to convert the kinetic energy from wind into electrical energy. As we know that, wind turbines can be generally divided into two configurations: horizontal-axis wind turbine (HAWT) and vertical-axis wind turbine (VAWT). HAWT is usually more efficient and has a longer lifetime than VAWT configuration [1]. Therefore, vast majority of the large-scale wind turbines are applied as horizontal-axis designs. Traditional utility-scale HAWTs have one singular rotor with three rotating blades, and most of them are mounted in front of turbine tower. This upwind configuration is mainly for the consideration of aerodynamic performance, for instance, to reduce the tower shadow effect [2–4], etc. However, the disadvantages of this design are also prominent. Take the rotor blades as an example, the rotor has to be positioned far enough away from the turbine tower to avoid blade strike. Therefore, these rotor blades have to be designed as inflexible as possible to avert such problems, especially for the blades employed in MW-class wind turbines. As a result, this requirement would greatly increase the blade manufacturing cost. It is massive especially compared with the numerous turbines (By the end of 2016, the global cumulative installed wind power capacity expanded to 486,749 MW) [5] installed in large-scale onshore and offshore wind farms. In order to avoid blade strike occurring in the operation, people usually tilt the rotors (e.g., 2.5–8°) slightly to keep them away from turbine towers [2,3,6,7], but which would reduce the power generation in comparison to those turbines with zero tilt angle [8]. In addition, upwind wind turbines require a complicated yaw control system to keep the turbine rotor facing the incoming wind [9]. With the concerns of these drawbacks, the downwind configuration was

* Corresponding author.
E-mail address: huhui@iastate.edu (H. Hu).
[1] Current address: Simulation Innovation and Modeling Center (SIMCenter), The Ohio State University, Columbus, OH 43210, USA.

https://doi.org/10.1016/j.enconman.2018.02.038
Received 2 November 2017; Received in revised form 18 January 2018; Accepted 9 February 2018
Available online 22 February 2018
0196-8904/

Nomenclature

A	area of blade rotational disk [m^2]
C_P	power coefficient [–]
C_T	thrust coefficient [–]
D	diameter of turbine rotor [m]
H	turbine hub height [m]
I_u	turbulence intensity [–]
P	power output [W]
Re_D	Reynolds number based on rotor diameter [–]
TKE	turbulent kinetic energy [m^2/s^2]
TSR	tip-speed-ratio [–]
U_H	freestream velocity at turbine hub height [m/s]
α	power law exponent [–]
σ_u	root-mean-square of the turbulent velocity fluctuation [m/s]
η	efficiency of DC generator [–]
θ	blade phase angle [°]
ω_y	vorticity (out of plane) [1/s]

proposed to overcome these disadvantages existing in the upwind design [4]. As we know that, the rotor in the downwind configuration is installed behind turbine tower, which means the rotor blades can be designed more flexible since there is no danger of blade strikes. This could largely reduce the manufacturing cost and lower the weight of rotor blades, potentially resulting in a 15–20% reduction in turbine capital cost [10]. In addition, if nacelle can be appropriately designed to follow the incoming wind direction passively, there is no need to use a yaw control mechanism in the wind turbine system.

In comparison to a large amount of studies conducted to investigate the flow performance on traditional upwind HAWTs [11–15], relatively little attention is paid on the downwind design for commercial application possibly due to the concern of shadow effect. Because people found shadow effect would reduce the total power coefficient and increase turbulence and fatigue on wind turbines [2]. As a result, very few literatures on investigating downwind turbines can be found in the past several decades and the corresponding flow characteristics are still not quite clear. Therein, most of them were studied by computational methods. Janajreh et al. [16,17] numerically investigated the rotor-tower interaction of downwind turbine configuration. They found that the aerofoil shape tower has a lower resulting aerodynamic force on rotating blades and a reduced rotor wake in comparison to those in the circular tower case. However, these advantages would be diminished under highly-turbulent flows. Zhao et al. [9] used a high-fidelity CFD code U^{2}NCLE to compare two-bladed and three-bladed upwind and downwind turbines, respectively. They stated that the unsteady aerodynamic loads are higher in the downwind turbine than those in the upwind turbines, but the impact of rotor orientations (i.e., upwind or downwind) are smaller than that caused by the blade number and the rotating speed. Zhou and Wan [18] also observed that the rotor-tower interaction in downwind turbines would cause a larger thrust reduction when the rotating blades approaching turbine tower. Given that a higher flow incidence across the rotational disk and a higher axial velocity in the outboard portion of rotor blades, Frau et al. [7] found a 3% enhancement of power coefficient in the downwind configuration. However, the drawback is that the loadings on rotor blades are 14% higher than that in the upwind design. In contrast with the numerical studies on the downwind turbines, Kress et al. [6] conducted an experimental investigation to understand the unsteady torque characteristics with different rotor cone angles. They observed that the unsteadiness of rotor torque for the downwind configurations is about 38–68% higher than the values in the corresponding upwind designs, which is similar with the results shown in the aforementioned computational studies. Larwood and Chow [19]confirmed this finding through a wind tunnel study on a downwind NREL Phase VI wind turbine. However, the fatigue loads can be significantly mitigated if an aerodynamic shroud that aligned with the incoming wind direction, is amended on the turbine tower. They also stated that the downwind coning could essentially reduce the average loads for blade flapbending, which shows a great benefit in applying the downwind design for large-scale wind turbines. Furthermore, Kress et al. [20] found the downwind rotor configuration is more suitable for yaw stability with a given wind condition, which could be easier to control turbine rotors and produce more power from the same incoming airflow.

According to the aforementioned studies, the flow characteristics of downwind rotor design, such as the rotor-tower interaction, are not fully understood because the shortage of detailed investigations. As a result, the aim of the present study is to provide a comprehensive experimental study on the flow performance of a traditional upwind turbine (UWT) and a downwind turbine (DWT). The instantaneous wind loads acting on both wind turbines were measured to quantify the fatigue analysis. The detailed velocity distributions were obtained by a planar particle image velocimetry (PIV) measurement, under the same incoming flow condition. The measured velocity and vorticity distributions were used to characterize the turbine wake characteristics and evolutions of the unsteady blade tip and root vortices. The power outputs of the model wind turbines were also measured to quantify the influence of upwind and downwind configurations in power generation.

2. Experimental setup and wind turbine models

2.1. Wind tunnel

The experimental study was conducted in a large-scale Atmospheric Boundary Layer (ABL) wind tunnel with the dimension of 20.0 m × 2.4 m × 2.3 m in the test section [21]. It is a closed-circuit wind tunnel with the capacity of generating a maximum ABL wind speed of 45 m/s and the side walls in the test section are transparent. Fig. 1 shows the wind tunnel test section and a conventional upwind HAWT model is mounted at the center of the ground. A series of aluminum chain arrays, which are perpendicular to the flow direction (i.e., x-direction) and with an equal spacing of 15-inch, are placed in the test section in order to generate an incoming airflow with an ABL profile usually seen in offshore wind farms. The wind tunnel ceiling can be adjusted to ensure the boundary layer growth under approximately zero pressure gradient in the streamwise direction. Further information of this wind tunnel in generating ABL wind profiles can be found in the

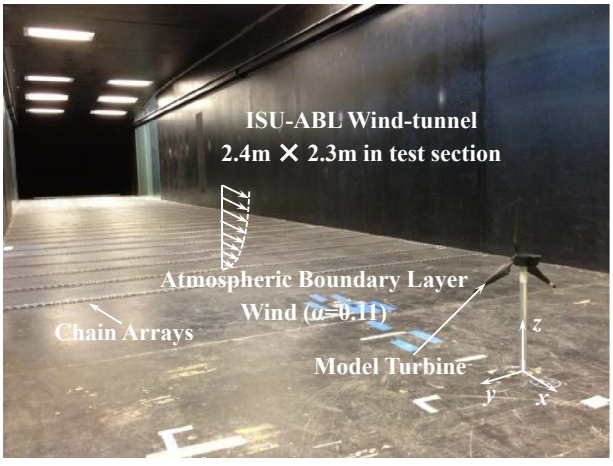

Fig. 1. The HAWT model and the test section of wind tunnel.

previous study of Tian et al. [22].

A typical wind profile over an open terrain condition can be approximately expressed as a power law function [23]. For the present study, the incoming wind speed in vertical direction ($U(z)$) can be determined by the function shown below:

$$U(Z) = U_H(z/H)^{\alpha} \quad (1)$$

where U_H is the wind speed at the turbine hub height H and the exponent 'α' in this equation is determined by surface roughness. As we know that, the incoming airflows in offshore wind farms have relatively lower turbulence levels in comparison to those in onshore terrains, because the surface roughness of ocean surfaces is rather smaller. Turbines operated in typical offshore wind farms (e.g., the Greater Gabbard in UK and Horns Rev II in Denmark) are usually facing an ABL wind profile with the exponent of $\alpha \approx 0.10$ [24]. Hsu et al. [25] also recommended an exponent of $\alpha \approx 0.11$ for offshore terrains under neutral stability condition, which is similar to the value recommended by ISO standard [26]. Apart from the velocity profiles of incoming airflow, the turbulence intensity of the wind profiles is another essential parameter to be determined. Tong [27] suggested that a range from 8% to 12% is usually used at the hub height of offshore wind turbines to represent the typical uncertainties of incoming airflows. Fig. 2 shows the streamwise velocity and its turbulence intensity profile used for the current study, which were measured by using a high-resolution anemometry system at the location where the test model turbines were mounted. It should be noted that the streamwise velocity shown in Fig. 2(a) is normalized by the streamwise velocity (U_H) measured at the turbine hub height. By adjusting the ceiling height of the wind tunnel, the incoming velocity profile is found to be fitted very well to a power function plot with the exponent of $\alpha = 0.11$. The turbulence intensity (I_u) was also suitably set to 9.9% at the turbine hub height, which is defined as follows:

$$I_u = \sigma_u / \overline{U}_{local} \quad (2)$$

where σ_u is the root-mean-square of the fluctuations in streamwise velocity, and $\overline{U}_{local}$ is the time-averaged streamwise velocity where the anemometer is located. Both of the wind speed and the turbulence intensity profiles are suitably located within the ranges as suggested by Hsu et al. [25] and Tong [27].

2.2. Wind turbine models

In this study, two model wind turbines (UWT and DWT) were constructed for the comparative investigations. The UWT shown in Fig. 3(a), represents the most widely-used three-blade HAWT deployed in large-scale wind farms. The detailed design parameters of this model turbine can be found in our previous studies [21,26,28]. As a contrast, Fig. 3(b) shows the schematic of the DWT, which has the same size in rotor and the same distance between the rotor and turbine tower. For DWT configuration, due to the turbine rotor is placed behind the nacelle, there is another cone hub installed in front of the downwind rotor to minimize the blockage effect from the nacelle. The rotational direction of UWT and DWT was kept as the same during the operation. The diameter of turbine rotor (D) is 0.28 m and the height of turbine hub (H), namely, the distance between the ground and the turbine hub, is 0.225 m for all model turbines. The model turbines (with a scaled ratio of 1:320) were designed to mimic a conventional utility-scale HAWT with the rotor diameter of 90 m and turbine hub height of 80 m sited in the typical offshore wind farms. The rotating blades, hubs and nacelles, were fabricated through a rapid prototyping machine by using stiff plastic materials. The blockage ratio in the test section was calculated to be around 1.2%, thus, the blockage effect can be omitted in the measurements [29].

During the test, the incoming streamwise velocity at the hub height was adjusted to be around 6.5 m/s (i.e., $U_H = 6.5$ m/s). Therefore, based on the wind speed at hub height and the rotor diameter, the corresponding Reynolds number ($Re_D = U_H D/\nu$) was calculated to be around 1.2×10^5. Obviously, this value is much lower than those of utility-scale HAWTs ($Re_D > 1.2 \times 10^7$) operated in large-scale wind farms [30]. According to the studies conducted by Hu et al.[31], Whale et al.[32], Alfredsson et al.[33] and Medici & Alfredsson[34], while Reynolds number of a wind turbine may have a significant effect on the power production performance of the wind turbine (i.e., the maximum power coefficient would be much lower for a small-scale model turbine operating at a lower Reynolds number), the wake characteristics and the evolution of the unsteady vortices in the turbine wake would become almost independent of the chord Reynolds number when the chord Reynolds number of the model turbine is higher enough. Chamorro et al. [35] found that, the flow characteristics in turbine wakes,

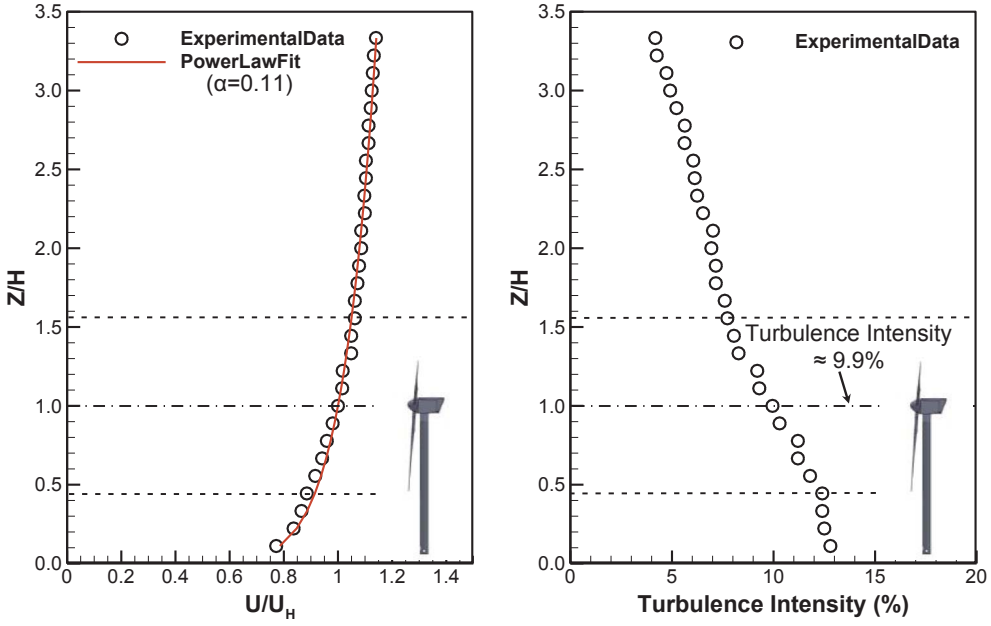

(a) Streamwise velocity profile (b) Turbulence intensity profile

Fig. 2. ABL wind profiles used in the experiments.

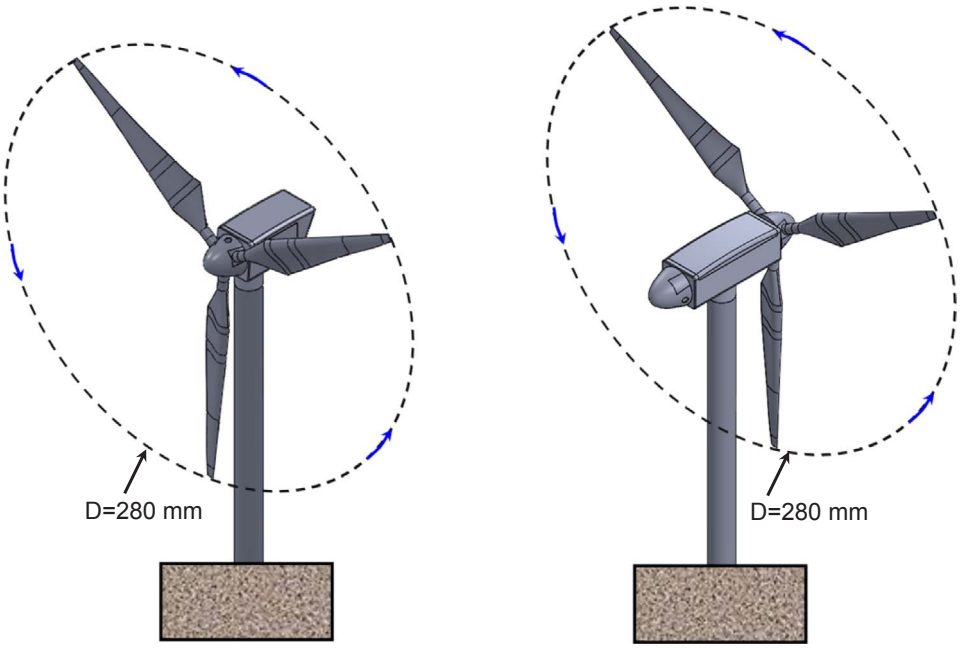

Fig. 3. Schematics of the tested wind turbine modles.

such as velocity, shear stress and turbulence intensity, were found to illustrate asymptotic manners with the changing of the Reynolds numbers. While the independence of Reynolds number for velocity was found to be reached at a lower value of $Re_D \approx 4.8 \times 10^4$, the Reynolds number independence would reach at $Re_D \approx 9.3 \times 10^4$ for higher order characteristics (e.g., shear stress and turbulence intensity). As mentioned above, the corresponding Reynolds number of the present study is about 1.2×10^5, which is well above the required minimum Reynolds number for the independence for both low and high orders flow characteristics as suggested by Chamorro et al. [35]. Similarly, the studies of Whale et al. [32] and Medici et al. [36] also revealed that, the behaviors of the unsteady flow structures in the turbine wake would become independent to the Reynolds number once it reaches to a certain level. The wind turbines would generate similar unsteady wake flow structures under the same tip-speed-ratio (TSR).

2.3. Dynamic wind load and power output measurements

During the experiment, the wind turbine blades, hubs and nacelles were assembled together and supported by a circular rod that was

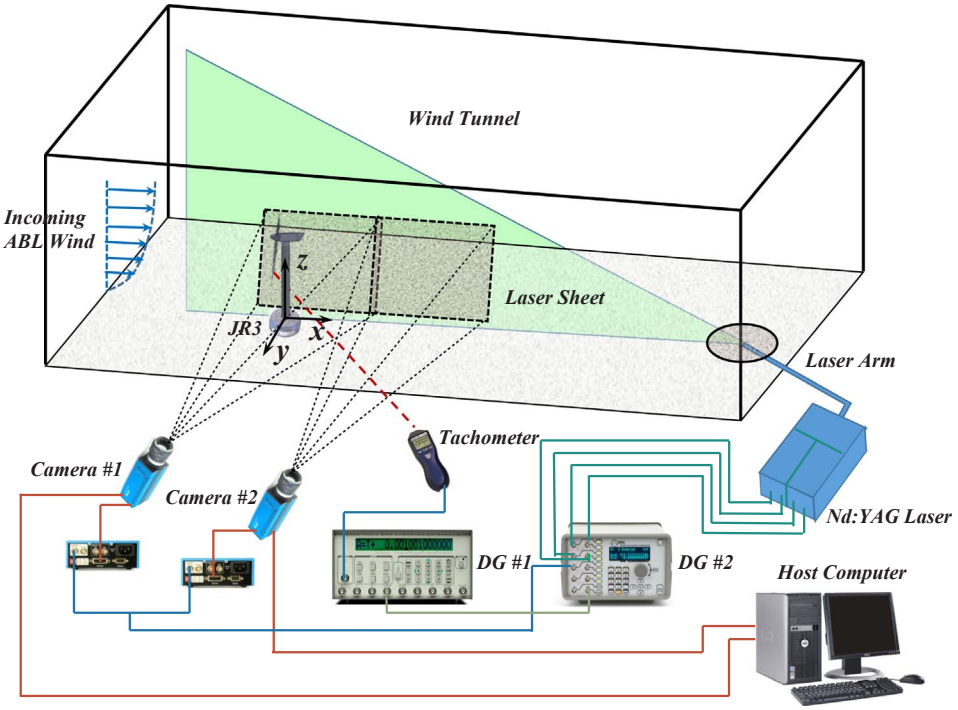

Fig. 4. Experimental setup for the dynamic wind loads and PIV measurements.

employed as a turbine tower. In order to monitor the dynamic wind loads acting on the wind turbines, a load cell called JR3 (model: 30E12A-I40), was applied to measure the dynamic thrust forces and bending moments through a high-sensitive force transducer. The details about this load cell are available in our previous research [26]. Fig. 4 shows the experimental setup for the wind load measurement. The load cell was mounted under the wind tunnel test section to support the turbine tower. During the measurements, the aerodynamic forces acting on these model turbines were continuously collected for 120 s with a sampling rate of 1000 Hz for each model wind turbine. A Monarch tachometer was adopted to capture the turbine rotational speeds. It should be noted that the resonant frequencies measured from the load cell were found to be essentially higher than the rotational frequencies of turbine rotors.

The power outputs of the model wind turbines can be calculated through measuring the voltages from the DC generator in the nacelle and the currents in the electric circuits. By adjusting the electric resistance in the circuits, the wind turbine rotational speed can be varied from 0 to 2200 rpm, which are equivalent to the TSR from 0 to 6.5. The optimum TSR (i.e., with the maximum power output) was observed to be around 5.0 in the current study, which lies in the range of 4.0–8.0 for typical modern wind farms [37].

2.4. Flow field measurements

Fig. 4 also illustrates the experimental setup for the 2-D PIV measurements, which was used to measure the velocity fields at the vertical central plane (i.e., $Y = 0$) to quantify the flow characteristics in the turbine wakes ($X/D < 2.2$). A fog machine (ROSCO 1900) was used to generate small oil droplets (~1 μm in diameter) and spray them in the incoming airflow for illumination purpose. A double-pulsed Nd:YAG laser (EverGreen 200) was utilized to produce a pulsed laser beam at a wavelength of 532 nm. The laser beam was then formed as a sheet with a thickness of around 1.0 mm after passing through a series of mirrors along with cylindrical and spherical lenses. Two high-resolution 14-bit CCD cameras (PCO2000), with an overlapping capture window of 20 mm in streamwise direction, were placed perpendicular to the laser sheet for image acquisitions simultaneously, because the window size of one camera is not sufficient to capture the whole interested region in the near wake. A digital time delay generator (BNC565) was applied to control the timing sequences of the laser system and the image acquisition. After the image acquisition, the instantaneous velocity components can be derived from the measured PIV snapshots in the post-processing by using a cross-correlation with an interrogation window of 32 × 32 pixels and an effective overlap rate of 50%. The ensemble-averaged flow characteristics such as mean velocity, turbulent kinetic energy (TKE) and vorticity can be calculated from the velocity components and their variances. For each test case, a sequence of 1000 pairs of instantaneous images were captured so as to attain a good convergence of flow characteristics of the ensemble-averaged measurements. The uncertainty levels of measurements were estimated to be around 2% for velocity and 5% for TKE and vorticity, respectively [38].

Both ensemble-averaged and phase-locked PIV measurements were performed to achieve the time-averaged and instantaneous flow fields. During the ensemble-averaged measurements, a constant image acquisition rate (different from the blade rotating frequency) was utilized to measure the flow quantities in the wake region under variant blade phase angles. While for the phase-locked measurements, a digital tachometer and another time delay generator (Stanford DG535) were employed in the system to control the timing of image acquisition at a specific blade phase position. They were performed to elucidate more insights about the evolution of unsteady turbulent structures such as tip and root vortices shedding from different blade phase positions. During the measurement, the zero phase angle was pre-selected at the most upward position of a rotor blade, which was also marked by a reflective tape on the blade surface. Since the turbine rotor has 3 blades (with a phase differentiation of 120°), 8 phase angles were selected ranging from 0° to 105° with a constant increment of 15°. At each selected blade phase angle, 400 image pairs were captured to calculate the phase-averaged flow statistics in the wake regions.

3. Results and discussion

3.1. Measurements of dynamic wind loads acting on the wind turbines

The effect of dynamic wind loads acting on turbine is important in the optimal design of large-scale HAWTs [31]. In this study, the instantaneous force components were measured by a JR3 load cell with a sampling frequency of 1000 Hz. The corresponding thrust coefficient (C_T) of wind turbines, are defined as

$$C_T = \frac{T_x}{\frac{1}{8}\rho U_H^2 \pi D^2} \tag{3}$$

where T_x is the thrust force component in x direction (i.e., streamwise direction), ρ is the density of incoming airflow. Fig. 5 illustrates the instantaneous thrust coefficient, the time-averaged results are also plotted as red dashed lines.

Fig. 5 shows the time sequences of the instantaneous thrust acting on the model wind turbines in terms of thrust coefficient (C_T) in a continuous 120-s measurements (only one out of every 10 original measurement data being shown in the plots). The instantaneous thrust forces are found to be highly fluctuated during the test, which could be

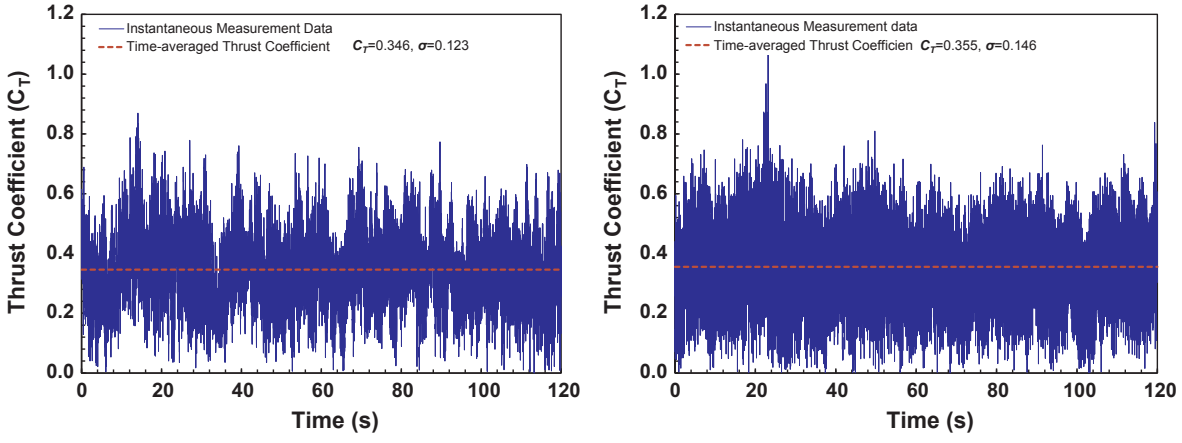

Fig. 5. Measured thrust coefficients.

2 times higher than the time-averaged values. The time-averaged thrust coefficient of UWT model is measured to be 0.346, which is close to the values reported in the experimental studies of Lebron et al. (0.32) [39], Cal et al. (0.32) [40], and Zhang et al. (0.48) [41] under similar tip-speed-ratios (TSR). However, the thrust coefficient values in computational studies are usually found to be much higher than those in the experimental investigations. For example, Wu and Porte-Agel [42] found the thrust coefficient was about 0.75 at the TSR near 5.0 due to a much higher Reynolds number used in their study. For downwind configuration, as expected, both of the mean thrust coefficient and its standard deviation (σ) values are found to be higher than those in the UWT model, which agree well with the findings shown in Zhao et al. [9] and Frau et al. [7]. The thrust coefficient is found to be slightly enhanced (0.355 versus 0.346) by 2.6%, while its fluctuation (i.e., standard deviation) increases by 18.7%. The majority of instantaneous thrust coefficients for the UWT case are found to be within the range between 0.20 and 0.55, while for the DWT case, the majority of them are observed to be concentrated from 0.15 to 0.60. As suggested by Hu et al. [31] and Tian et al. [22], the standard deviation values of the dynamic wind loads can be employed as an essential parameter to evaluate the fatigue loads acting on wind turbines. The larger variations (i.e., with high fluctuations) of wind loads in the DWT configuration would indicate greater fatigue loads acting on the turbine, which is believed to be due to the shadow effect occurred between the turbine tower and rotor blades. Although the mean thrust coefficients for both compared configurations are almost identical, the larger fluctuations may indicate a less lifetime of the DWT configuration. In addition, according to the description in Troldborg et al. [43], the shadow effect in the downwind design would also cause power reduction, which will be discussed in the following section of power measurement analysis.

3.2. Power measurements

In order to evaluate the drawback of DWT configuration in power generation due to the shadow effect, the power coefficient of the two wind turbines was also measured for comparison. It is well known that, the Reynolds number in such small-scale wind turbines is much lower than that of the utility-scale ones, which has a substantial effect on the power generation in wind-tunnel testing [31]. In the present study, the power coefficient (C_P) is defined as follows:

$$C_P = \frac{V^2\eta}{\frac{1}{2}\rho U_H^3 A R_L} \tag{4}$$

where R_L is the electric resistance applied in the circuit, V is the measured voltage of R_L, A is the blade rotational area and η is the efficiency of the small DC generator. As described in Hu et al. [31], the maximum power coefficient of wind turbines operating at low Reynolds number could be significantly lower than that of large-scale wind turbines in modern wind farms. In fact, the optimum mechanical power coefficient of the traditional UWT model was found to be about 0.2 for the present study, which is significantly lower than that of utility-scale HAWTs (e.g., C_P = 0.40–0.45) placed in modern onshore and offshore wind farms. Instead of comparing the absolute value of power coefficients directly, they were normalized based on the power coefficient (C_{P_ref}) of the traditional UWT system.

Fig. 6 gives the normalized power coefficients of the UWT and DWT models with the same incoming flow condition. As expected, the power generated from the DWT model was found to be lower than that in the UWT model due to the shadow effect that results in a considerable velocity deficit and turbulent unsteady vortices behind the turbine tower. As a result, the incoming flow velocity would be much lower and the turbulence level in the wake flow would be much higher in this region for the DWT case. It can be clearly seen from the results that only a 3.2% reduction is observed in the downwind configuration in comparison to the typical upwind design, which is slightly lower than the value (7.3%) in the computational study on a large-scale wind turbine with the same configurations [9]. The results obtained in the present study is close to the investigation in Larwood and Chow [19], they also found that there is no obvious evidence of lower power generation for a downwind design, only a mild difference existing at a high wind speed. It indicates that, the shadow effect has less impact on the power generation for the downwind configuration when compared with the effect in fatigue loads. Moreover, Yoshida et al. [44] and Reiso et al. [45] stated that if the downwind turbine system can be designed appropriately, the power output can be increased by mitigating the shadow effect when turbines were sited in some complex terrains.

3.3. PIV measurement results

As mentioned in the previous section of experimental setup, two cameras were employed in tandem to measure the whole interested regions. Fig. 7 shows the ensemble-averaged streamwise velocity distributions in the turbine wakes of the UWT and DWT systems ranging from $X/D = -0.2$ to $X/D = 2.2$, which are normalized by the incoming streamwise velocity at the turbine hub height (U_H). It should be noted that the velocity data shown in window #1 are captured by the first camera (the left side of the vertical dashed line) and the following ones shown in window #2 are measured by the second camera (the right side of the vertical dashed line). As expected, from the velocity comparison between the upstream and downstream regions of turbine rotor, large deficits are observed in the turbine wakes of both model wind turbines, indicating a significant portion of wind energy is harvested by the upstream wind turbines. There is an essential distinction can be found in the central turbine wake regions (e.g., $-0.2 < Z/D < 0.2$). From the comparison, a region teemed with high-momentum flow is found to occur over the nacelles for both cases because little to no wind energy is harvested in the region near blade root [26]. However, it is observed to travel to a further downstream location in the turbine wake of DWT design.

In addition, the velocity deficit in the wake of the UWT model is found to be greater than that in the DWT model, especially in the lower half turbine wake. This is because more kinetic energy from the incoming flow is harnessed by the upwind turbine rotor and is believed as the reason why UWT system generates a slightly higher power output as shown in Fig. 6. Due to the existence of nacelle and turbine tower, the airflow is essentially affected and decelerated in the region of $0 < X/$

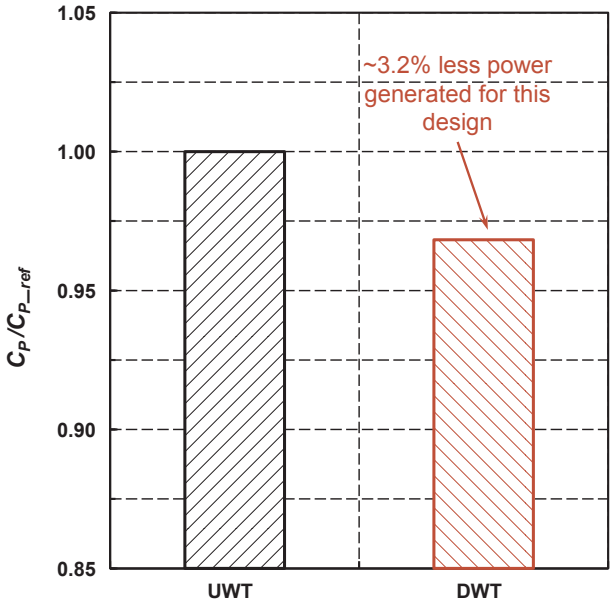

Fig. 6. Power measurement results of the UWT and DWT models.

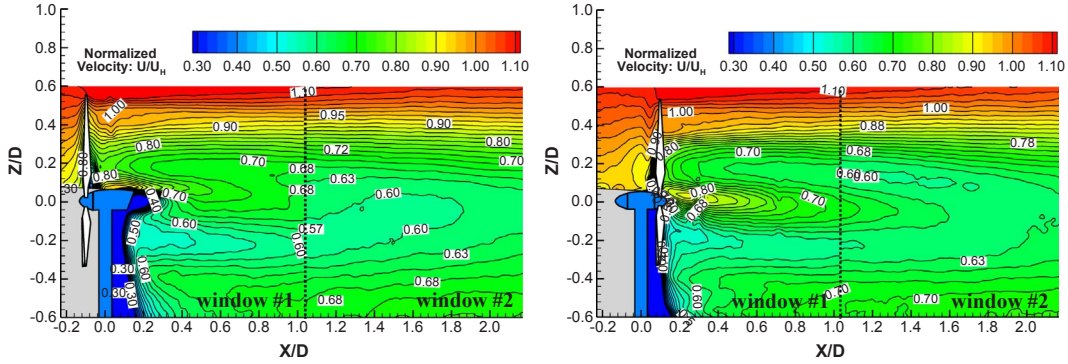

(a) UWT model (b) DWT model

Fig. 7. Ensemble-averaged streamwise velocity distributions in the turbine wakes.

$D < 0.2$ in the lower half turbine wake. While for the DWT case, the turbine blades are found to rotate in this low-momentum region as the blades in the shadow region of the turbine tower, which causes a much lower kinetic energy ($U/U_H < 0.3$) available in the incoming airflow for the downwind rotor. This low-momentum region would extend up to X/D ≈ 0.12 behind the turbine tower.

Fig. 8 shows the vertical profiles of streamwise velocity distribution extracted from the PIV measurement results given in Fig. 7 at the downstream locations of $X/D = 0.5$, 1.0 and 2.0, respectively. The profiles of the incoming ABL wind (i.e., for the case with no model wind turbines placed at the measuring locations) were also given in plots, which can be used as the baseline to reveal the evolution of the velocity deficits in the turbine wake flows. Due to the difference of rotor position, an essential differentiation can be identified at the downstream location of $X/D = 0.5$, as shown in Fig. 8(a). The velocity deficit in the region of $Z/D > 0.3$ in the wake of UWT model was found to be slightly larger than that in the DWT system. This is because a longer distance between rotor blade and the downstream position X/D = 0.5 for the upwind case could help to recover the streamwise velocity at a higher level. A larger velocity deficit is also found in the region of $-0.2 < Z/D < 0.1$ behind the UWT model, this is more related to the effect induced by root sections and nacelle. While in the lower half turbine wakes ($Z/D < -0.2$), the streamwise velocity distributions are almost identical from near wake ($X/D = 0.5$) to far wake ($X/D = 2.0$) regions. Compared with the significantly higher force fluctuations induced by the shadow effect, only very little differences were observed in the turbine wake flows. While differentiations in the streamwise velocity profiles for the two compared cases can still be found at the downstream location of $X/D = 1.0$, the differences were found to become much smaller, in comparison to those at the upstream location of $X/D = 0.5$. Only very little changes can be identified in the compared turbine wakes at the further downstream location of $X/D = 2.0$.

In order to provide further insights in the turbulent flow characteristics in the turbine wakes, the in-plane distribution of normalized turbulent kinetic energy (TKE) is derived from the measured flow fields, which is defined as below:

$$TKE = \frac{1}{2}(\overline{u'^2} + \overline{w'^2})/U_H^2 \tag{5}$$

where u' and w' are the variations of streamwise and vertical velocity, respectively. Fig. 9 illustrates the in-plane TKE distributions in the cases of UWT and DWT. It can be seen clearly that, the TKE distributions have a significant differentiation in the lower half turbine wake. Very high TKE levels (with red color) are concentrated in a region just right behind the nacelle and turbine tower (up to $X/D \approx 0.4$), which is closely related to the formation and shedding of the highly-turbulent root, nacelle and tower vortices. Similar structures and magnitudes of the flow characteristics were also observed in the studies of Tian et al.[22] and Jin et al.[46]. However, the region with similar high levels of TKE shown in Fig. 9(b) is much smaller than that illustrated in Fig. 9(a), indicating the TKE levels behind the turbine tower are significantly mitigated due to the existence of downwind rotor. According to the

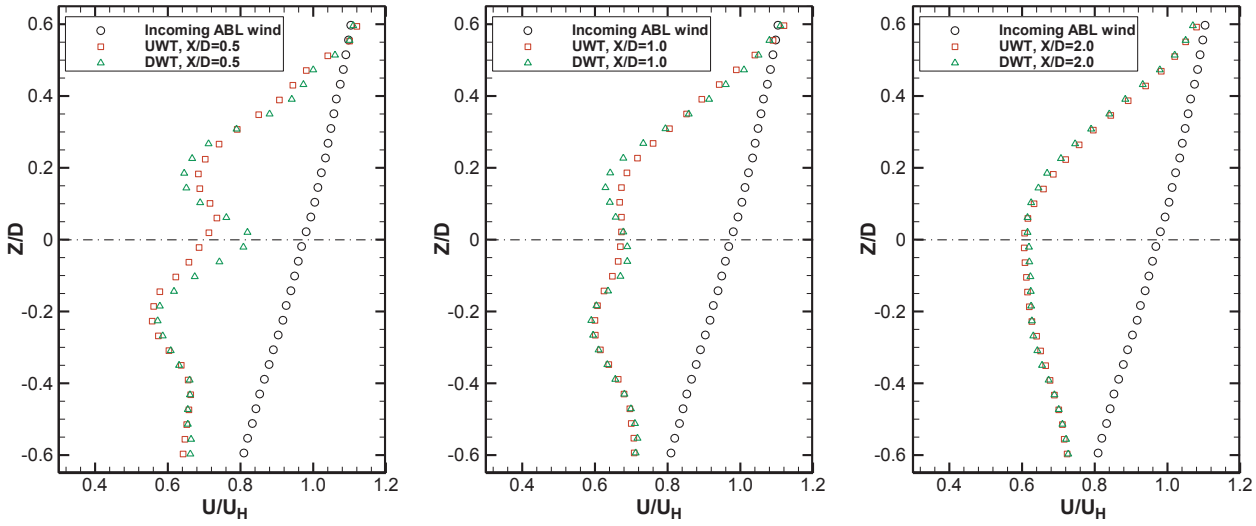

(a) X/D=0.5 (b) X/D=1.0 (c) X/D=2.0

Fig. 8. Vertical profiles of streamwise velocity in the turbine wakes.

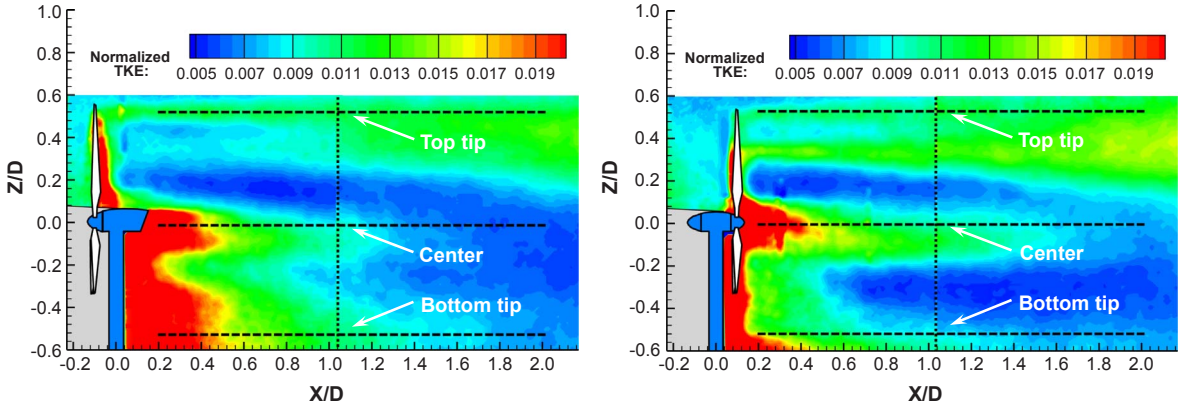

Fig. 9. Turbulence Kinetic Energy (TKE) distributions in the turbine wakes.

results shown in Fig. 7, when the turbine blades rotate approaching the tower, they are operated in a flow not only with very low-momentum but also with extremely high unsteadiness. This could be a good explanation for the higher dynamic wind load fluctuations in the DWT configuration shown in Fig. 5.

For the upper half turbine wake, the region with high TKE levels is found to appear in the shedding path of tip vortices. The TKE levels are observed to gradually increase from near to far wake regions, which also confirms with the findings reported in Lu and Porte-Agel [47] and Yang et al. [48]. Fig. 9(b) depicts a slightly higher magnitude within the region of $0.4 < Z/D < 0.6$ in the DWT model, indicating similar strength and structures of vortices shedding from the blade tips. But a second row of high levels of TKE is found to occur in the region of $0.25 < Z/D < 0.4$, which may imply a series of vortices also shedding from the mid-section of rotating blades. In order to provide a more quantitative comparison, the TKE levels at three paths (i.e., top tip, center and bottom tip shown in Fig. 9), were also extracted from near to far wake regions from the PIV measurements. Fig. 10 presents the TKE profiles from $X/D = 0.2$ to $X/D = 2.0$ at these three paths. It can be seen clearly that, the distributions of TKE in the shedding path of tip vortices (i.e., top tip) are quite close in the turbine wakes of the UWT and DWT models. However, the TKE values in the UWT case are found to be almost kept at a same level, while in the DWT case, the TKE values are observed to be increased slightly from near wake to far wake regions. Compared to the TKE levels at the other two paths (center and bottom tip), they are found to be the lowest in the near wake region ($X/D < 0.6$) but with the highest level in the far wake regions ($X/D > 1.0$). In contrast, the TKE values in the paths of center and bottom tip decrease dramatically as the distance increases. As we can see from Fig. 7, very low-momentum flows existing in the region just right behind nacelle and tower, meanwhile, which also have very high-kinetic energy as shown in Fig. 9. Fig. 10 depicts a steep drop of TKE in the region of $X/D < 0.6$, and then a mild reduction beyond that region for both center and bottom tip paths. As suggested by Tian et al. [22], the TKE levels can be employed as an important parameter to indicate the turbulent mixing and velocity deficit recovery in the wake regions. Therefore, as illustrated in Fig. 8, the velocity deficit in the lower half turbine wakes is found to recover faster than that in the upper half wakes due to the stronger wake mixing in the downstream regions, especially in the region near the blade bottom tip in the UWT case.

In addition to the ensemble-averaged results shown above, the phase-locked measurements were also conducted in order to unveil the evolution process of the unsteady flow structures in the wakes. As mentioned above, a rotor blade was labeled to record the phase angles during the measurement, and the zero phase angle was set to when this blade at the most upward position (i.e., PIV measurement plane). A digital tachometer, shown in Fig. 4, was utilized to monitor the rotational speed via the signals generated by the periodic pulses received from the labeled blade. Then, the laser and the camera systems were synchronized and triggered by these pulsed signals when the labeled blade position was assumed to be frozen at a certain time. The vorticity (ω_y) in the PIV measurement plane (i.e., $Y = 0$) is defined as follows:

$$\omega_y = \frac{\partial w}{\partial x} - \frac{\partial u}{\partial z} \tag{6}$$

It is used to characterize the unsteady turbulent structures such as the formation, breakdown and dissipating processes of the vortices shedding from tip, root, and nacelle as well as turbine tower in the wake flows.

Fig. 11 presents the normalized vorticity ($\omega_y D/U_H$) distributions in the vertical central plane of the UWT and DWT models. As we can see that, the flow characteristics are very complex, and a series of unsteady vortices are generated from the rotor blades, roots and nacelles as well as towers with various orientations and sizes. It should be mentioned that the increment of blade phase angle is set to 15°, but there are only four phase angles ($\theta = 0.0°, 30.0°, 60.0°, 90.0°$) presented in this paper for conciseness. As shown in the figure, the wake region can be divided into four zones, from top to bottom, which are dominated by the vortices shedding rotating blades, roots, nacelle and tower, respectively. Obviously, the vortices depicted in the upper half turbine wakes are much clear than those in the lower half turbine wakes in both cases. This indicates that the airflows in the lower half turbine wakes are significantly affected by the turbulent mixing effect from tower, nacelle and rotating blades in the vertical PIV measurement plane, instead of only being determined by the rotating blades as shown in the upper half wake regions. During the measurements, the tip vortices are found to be induced from the labeled blade tip at the phase angle of $\theta = 0.0°$. With

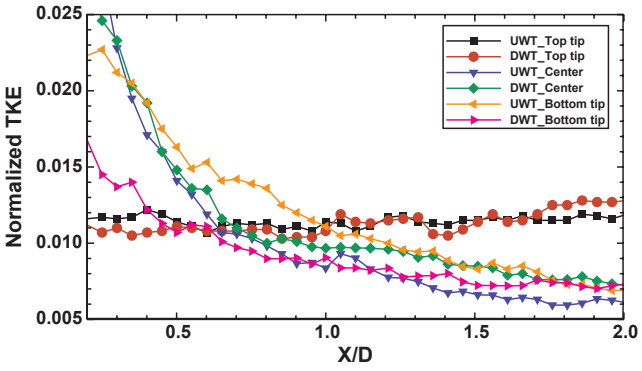

Fig. 10. TKE profiles extracted from the PIV measurements.

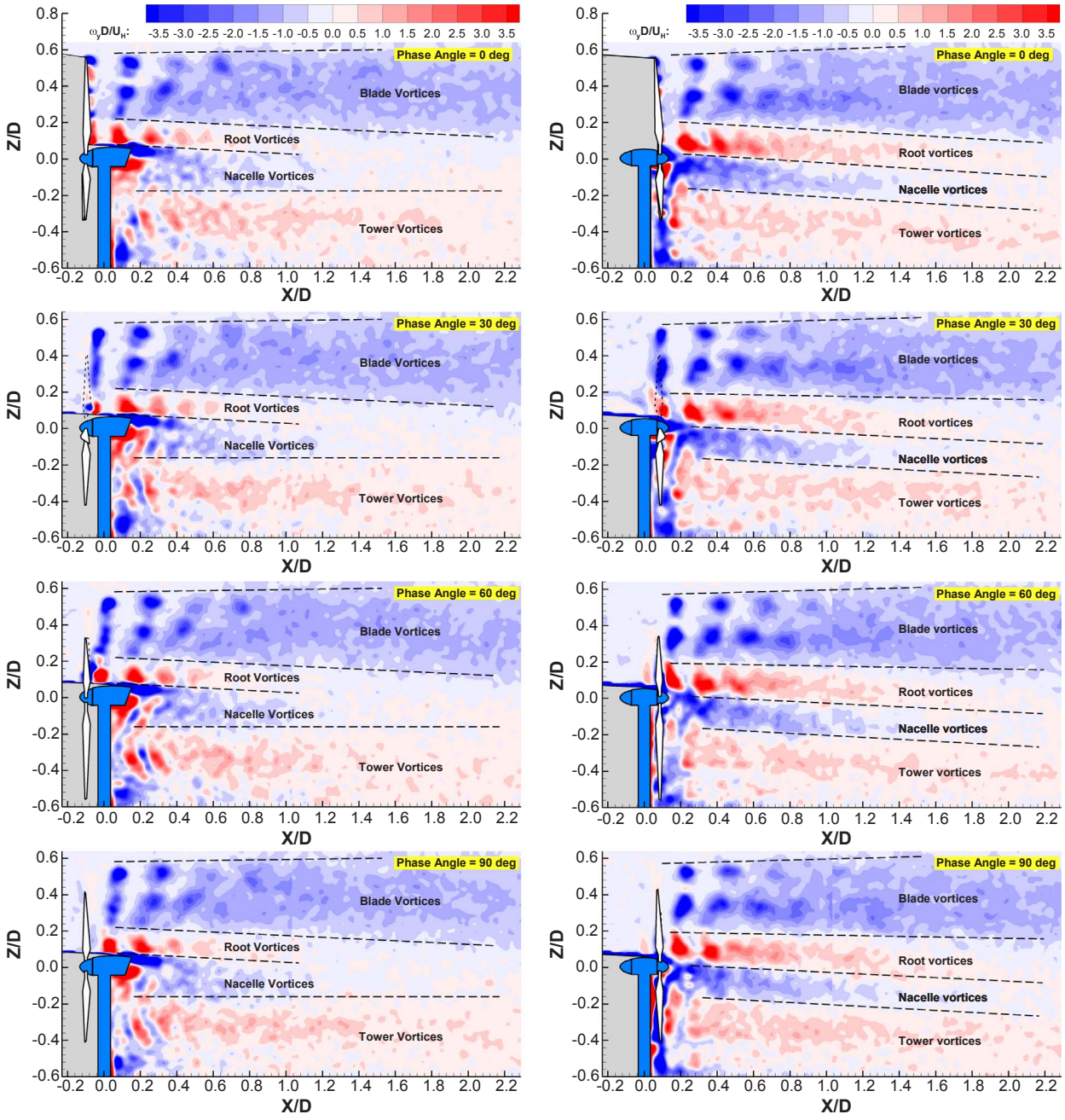

Fig. 11. Phase-locked PIV measurement results in the wake flows.

the phase angle increases, these tip vortices are observed to shed downstream and align sequentially with the other tip vortices shedding from the other two rotor blades in the wake regions. The shape and strength of the tip vortices in the turbine wakes of the UWT and DWT designs are observed to be quite similar.

Apart from the tip vortices, an additional row of vortices with high strength are also observed shedding from 60 to 70% spanwise of the rotor blades. This is believed due to the effect of low Reynolds number of the scaled turbine model to cause laminar flow separation at the locations. Similar vortex structures were also reported in the studies of Whale et al. [32] and Hu et al. [31]. As can be seen from Fig. 11, they are found to move outward mildly in the wake of the UWT model but slightly move inward in the wake of the DWT system. The strength of these vortices shed from the DWT system is also observed to be higher than those in the UWT model, which makes these vortices breaking down and dissipating at a further downstream location. The reason for these distinctions could be caused by the blockage effect from the nacelle and tower in the DWT model, which incurs the flow changing in spanwise (cross) direction. Recall the higher levels of TKE in the region of $0.25 < Z/D < 0.4$ in the turbine wake of the DWT model, they are associated with the stronger vortices shed from the corresponding sections of rotating blades. In addition to the vortices shed from the blade tip and outboard section (i.e., 60–70% spanwise), a series of vortices with opposite rotational direction are observed to shed from the root section. In Fig. 11(a), the root vortices are found to shed with circular shape and to dissipate rapidly in the near turbine wake. While in the DWT case, they are elongated in vertical direction and are found to dissipate finally at further downstream location, which is consistent with the higher TKE levels shown in Fig. 9(b) in the same region. Due to the existence of the turbine tower, the vortices in the lower half turbine

wake are not as distinct as those in the upper half wake. However, the rotor installed at upwind or downwind position changes the Karman vortex streets shedding from the turbine tower. They are found to be generated clearly and shed gradually in the upwind configuration, but which are broken down quickly by the rotating blades in the DWT design. It may cause the lower TKE levels in the lower turbine wake shown in Fig. 9(b).

4. Conclusion

A comprehensive experimental study was conducted in a large-scale wind tunnel to investigate the aeromechanic performance of a wind turbine with downwind configuration (i.e., DWT in short), in comparison with that of a traditional upwind wind turbine (UWT) design. The dynamic wind loads and the power coefficients of the model wind turbines were measured in an atmospheric boundary layer wind profile under a neutral stability condition. A high-resolution PIV system was also employed to perform both ensemble-averaged and phase-locked measurements to characterize the evolution of turbulent flow structures in the turbine wake regions. Based on the results derived from the present study, the conclusions can be summarized as follows:

(1) The dynamic wind loads acting on the wind turbine models were found to fluctuate greatly. The time-averaged thrust coefficient of the DWT model is slightly enhanced by 2.6% compared with that of the UWT system, while its fluctuation is found to increase by 18.7%, indicating much greater fatigue loadings acting on the DWT model due to shadow effect occurred between the turbine tower and rotor blades.
(2) The power coefficient of the DWT design is measured to be only 3.2% lower than that measured from the typical UWT model, which confirms with the findings reported in previous literatures.
(3) The PIV measurement of ensemble-averaged velocity field shows that the velocity distributions in the region of $Z/D > 0.2$ for both turbine are almost identical, but there is an essential distinction can be found in the central turbine wake regions ($-0.2 < Z/D < 0.2$). This region is observed to fill with high-momentum flow and travel to a further downstream location in the wake of DWT design. In addition, the velocity deficit in the upper half turbine wake in the UWT model is found to be greater than that in the DWT model, which is because more kinetic energy from the incoming airflow is harvested by the upwind turbine in the UWT design.
(4) The TKE distribution results illustrate that the turbine rotor in the DWT design is operated in a flow with very low-momentum and with extremely high unsteadiness, which could be a good explanation for the higher dynamic wind load fluctuations in the DWT shown in the force measurement.
(5) The phase-locked PIV measurement reveals that the turbulent flow structures in the turbine wakes are very complex. The vortices in the upper half turbine wakes are much more clearly identified than those in the lower ones since they are mainly determined by the rotating blades. Apart from the small distinction existed in tip vortices, an additional row of vortices with high strength are observed shedding from 60–70% spanwise of the rotor blades, which is believed to be due to the effect of laminar flow separation associated with the low Reynolds number in these scaled-down wind turbines. They are found to move outward mildly in the wake of the UWT model, but slightly move inward in the wake of the DWT design. The Karman vortex streets shedding from the turbine tower are found to be generated clearly and shed gradually in the upwind configuration, but which are broken down quickly via the interactions with the rotating blades in the downwind design.

While the findings derived from the present study are very helpful to elucidate the underlying physics for the development of novel wind turbines in either downwind or upwind configuration, much more comprehensive studies are still needed to explore/ optimize design paradigms for higher power yield and better durability of the wind turbines operating in complex atmospheric boundary winds.

Acknowledgements

The funding support from the Iowa Energy Center with Grant No. 14-008-OG and National Science Foundation (NSF) with Grant Numbers of CBET-1133751 and CBET- 1438099 is gratefully acknowledged.

References

[1] Wang Z, Zhuang M. Leading-edge serrations for performance improvement on a vertical-axis wind turbine at low tip-speed-ratios. Appl Energy 2017;208:1184–97. http://dx.doi.org/10.1016/j.apenergy.2017.09.034.
[2] Reiso M. The Tower Shadow Effect in Downwind Wind Turbines. 2013.
[3] Cai X, Gu R, Pan P, Zhu J. Unsteady aerodynamics simulation of a full-scale horizontal axis wind turbine using CFD methodology. Energy Convers Manag 2016;112:146–56. http://dx.doi.org/10.1016/j.enconman.2015.12.084.
[4] Loth E, Ichter B, Steele A, Selig MS, Moriarty PJ. Downwind Pre-Aligned Rotor for a 13.2 MW Wind Turbine. 33rd Wind Energy Symp 2015:1–8. doi:10.2514/6.2015-1661.
[5] Global Wind Statistics-2016. 2017.
[6] Kress C, Chokani N, Abhari RS. Design Considerations of Rotor Cone Angle for Downwind Wind Turbines. ASME Turbo Expo 2015 Turbine Tech Conf Expo 2015;138:1–13. doi:10.1115/1.4031604.
[7] Frau E, Kress C, Chokani N, Abhari RS. Comparison of performance and unsteady loads of multimegawatt downwind and upwind turbines. J Sol Energy Eng 2015;137:41004. http://dx.doi.org/10.1115/1.4030314.
[8] Abdelsalam A, Ramalingam V. Effect of the tilt angle on the wind turbine performance and wakes. Eighth Asia-Pacific Conf Wind Eng 2013;11.
[9] Zhao Q, Sheng C, Afjeh A. Computational aerodynamic analysis of offshore upwind and downwind turbines. J Aerodyn 2014;2014:1–13. http://dx.doi.org/10.1155/2014/860637.
[10] Koh JH, Ng EYK. Downwind offshore wind turbines: opportunities, trends and technical challenges. Renew Sustain Energy Rev 2016;54:797–808. http://dx.doi.org/10.1016/j.rser.2015.10.096.
[11] Ebrahimi A, Movahhedi M. Power improvement of NREL 5-MW wind turbine using multi-DBD plasma actuators. Energy Convers Manag 2017;146:96–106. http://dx.doi.org/10.1016/j.enconman.2017.05.019.
[12] Vaz JRP, Wood DH. Aerodynamic optimization of the blades of diffuser-augmented wind turbines. Energy Convers Manag 2016;123:35–45. http://dx.doi.org/10.1016/j.enconman.2016.06.015.
[13] Wang L, Tan ACC, Cholette M, Gu Y. Comparison of the effectiveness of analytical wake models for wind farm with constant and variable hub heights. Energy Convers Manag 2016;124:189–202. http://dx.doi.org/10.1016/j.enconman.2016.07.017.
[14] Nobari MRH, Mirzaee E, Nosratollahi M. Improvement of wind turbine performance using a novel tip plate structure. Energy Convers Manag 2016;123:592–609. http://dx.doi.org/10.1016/j.enconman.2016.06.078.
[15] Naderi S, Torabi F. Numerical investigation of wake behind a HAWT using modified actuator disc method. Energy Convers Manag 2017;148:1346–57. http://dx.doi.org/10.1016/j.enconman.2017.07.003.
[16] Janajreh I, Qudaih R, Talab I, Ghenai C. Aerodynamic flow simulation of wind turbine: downwind versus upwind configuration. Energy Convers Manag 2010;51:1656–63. http://dx.doi.org/10.1016/j.enconman.2009.12.013.
[17] Janajreh I, Talab I, MacPherson J. Numerical simulation of tower rotor interaction for downwind wind turbine. Model Simul Eng 2010;2010:1–11. http://dx.doi.org/10.1155/2010/860814.
[18] Zhou H, Wan D. Numerical investigations on the aerodynamic performance of wind turbine: downwind versus upwind configuration. J Mar Sci Appl 2015;14:61–8. http://dx.doi.org/10.1007/s11804-015-1295-9.
[19] Larwood SM, Chow R. Comparison of upwind and downwind operation of the NREL Phase VI experiment. J Phys Conf Ser 2016;753:22041. http://dx.doi.org/10.1088/1742-6596/753/2/022041.
[20] Kress C, Chokani N, Abhari RS. Downwind wind turbine yaw stability and performance. Renew Energy 2015;83:1157–65. http://dx.doi.org/10.1016/j.renene.2015.05.040.
[21] Wang Z, Ozbay A, Tian W, Hu H. An experimental study on the aerodynamic performances and wake characteristics of an innovative dual-rotor wind turbine. Energy 2018;147:94–109. http://dx.doi.org/10.1016/j.energy.2018.01.020.
[22] Tian W, Ozbay A, Hu H. Effects of incoming surface wind conditions on the wake characteristics and dynamic wind loads acting on a wind turbine model. Phys Fluids 2014;26:125108. http://dx.doi.org/10.1063/1.4904375.
[23] Jain P. Wind energy engineering. McGraw Hill Professional; 2007.
[24] Hansen KS, Barthelmie RJ, Jensen LE, Sommer A. The impact of turbulence intensity and atmospheric stability on power deficits due to wind turbine wakes at Horns Rev wind farm. Wind Energy 2012;15:183–96. http://dx.doi.org/10.1002/we.512.
[25] Hsu S, Meindl E, Gilhousen D. Determining the power law wind profile exponent under near neutral stability condition at sea.pdf. J Appl Meteorol 1994:757–65.
[26] Wang Z, Tian W, Ozbay A, Sharma A, Hu H. An experimental study on the

aeromechanics and wake characteristics of a novel twin-rotor wind turbine in a turbulent boundary layer flow. Exp Fluids 2016;57:150. http://dx.doi.org/10.1007/s00348-016-2233-6.
[27] Tong W. Wind Power Generation and Wind Turbine Design. WIT press; 2010.
[28] Wang Z, Hu H, Tian W, Ozbay A. An Experimental Investigation on the Wake Characteristics behind a Novel Twin-Rotor Wind Turbine. AIAA SciTech Conf 2015;AIAA 2015. doi:10.1115/1.4031476.
[29] Sarlak H, Nishino T, Martinez-Tossas LA, Meneveau C, Sorensen JN. Assessment of blockage effects on the wake characteristics and power of wind turbines. Renew Energy 2016;93:340–52. http://dx.doi.org/10.1016/j.renene.2016.01.101.
[30] Chamorro L, Arndt R, Sotiropoulos F. Turbulent flow properties around a staggered wind farm. Boundary-Layer Meteorol 2011;141:349–67. http://dx.doi.org/10.1007/s10546-011-9649-6.
[31] Hu H, Yang Z, Sarkar P. Dynamic wind loads and wake characteristics of a wind turbine model in an atmospheric boundary layer wind. Exp Fluids 2011;52:1277–94. http://dx.doi.org/10.1007/s00348-011-1253-5.
[32] Whale J, Anderson C, Bareiss R, Wagner S. An experimental and numerical study of the vortex structure in the wake of a wind turbine. J Wind Eng Ind Aerodyn 2000;84:1–21. http://dx.doi.org/10.1016/S0167-6105(98)00201-3.
[33] Alfredsson PH, Dahlberg J-A, Vermeulen PEJ. A comparison between predicted and measured data from wind turbine wakes. Wind Eng 1982;6:149–55.
[34] Medici D, Alfredsson P. Measurements on a wind turbine wake: 3D effects and bluff body vortex shedding. Wind Energy 2006;9:219–36.
[35] Chamorro L, Arndt R, Sotiropoulos F. Turbulent flow properties around a staggered wind farm. Boundary-Layer Meteorol 2011;141:349–67.
[36] Medici D, Alfredsson PH. Measurements on a wind turbine wake: 3D effects and bluff body vortex shedding. Wind Energy 2006;9:219–36. http://dx.doi.org/10.1002/we.156.
[37] Burton T, Jenkins N, Sharpe D, Bossanyi E. Wind Energy Handbook. 2nd ed. Wiley; 2011.
[38] Hu H, Wei T, Wang Z. An Experimental Study on the Wake Characteristics of Dual-Rotor Wind Turbines by Using a Stereoscopic PIV Technique. 34th AIAA Appl Aerodyn Conf 2016.
[39] Lebrón JR, Castillo L, Cal RB, Kang H, Meneveau C. Interaction Between a Wind Turbine Array and a Turbulent Boundary Layer. 48th AIAA Aerosp Sci Meet 2010:13.
[40] Cal RB, Lebrón J, Castillo L, Kang HS, Meneveau C. Experimental study of the horizontally averaged flow structure in a model wind-turbine array boundary layer. J Renew Sustain Energy 2010;2:13106. http://dx.doi.org/10.1063/1.3289735.
[41] Zhang W, Markfort CD, Porté-Agel F. Wind-turbine wakes in a convective boundary layer: a wind-tunnel study. Boundary-Layer Meteorol 2013;146:161–79. http://dx.doi.org/10.1007/s10546-012-9751-4.
[42] Wu YT, Porté-Agel F. Large-eddy simulation of wind-turbine wakes: evaluation of turbine parametrisations. Boundary-Layer Meteorol 2011;138:345–66. http://dx.doi.org/10.1007/s10546-010-9569-x.
[43] Troldborg N, Sørensen J. A simple atmospheric boundary layer model applied to large eddy simulations of wind turbine wakes. Wind Energy 2014;17:657–69. http://dx.doi.org/10.1002/we.
[44] Yoshida S. Performance of downwind turbines in complex terrains. Wind Eng 2006;44:487–501.
[45] Reiso M, Muskulus M. The simultaneous effect of a fairing tower and increased blade flexibility on a downwind mounted rotor. J Renew Sustain Energy 2013;5. doi:10.1063/1.4803749.
[46] Jin Z, Dong Q, Yang Z. A stereoscopic PIV study of the effect of rime ice on the vortex structures in the wake of a wind turbine. J Wind Eng Ind Aerodyn 2014;134:139–48. http://dx.doi.org/10.1016/j.jweia.2014.09.001.
[47] Lu H, Porté-Agel F. Large-eddy simulation of a very large wind farm in a stable atmospheric boundary layer. Phys Fluids 2011;23:65101.
[48] Yang X, Howard KB, Guala M, Sotiropoulos F. Effects of a three-dimensional hill on the wake characteristics of a model wind turbine. Phys Fluids 2015;27. doi:10.1063/1.4907685.